ACS Energy LETTERS

http://pubs.acs.org/journal/aelccp

LETTER

Quantifying the Capacity Contributions during Activation of Li_2MnO_3

Jatinkumar Rana,[¶] Joseph K. Papp,[¶] Zachary Lebens-Higgins, Mateusz Zuba, Lori A. Kaufman, Anshika Goel, Richard Schmuch, Martin Winter, M. Stanley Whittingham, Wanli Yang, Bryan D. McCloskey, and Louis F. J. Piper*

Cite This: *ACS Energy Lett.* 2020, 5, 634–641

Read Online

ACCESS | Metrics & More | Article Recommendations | Supporting Information

ABSTRACT: Though Li_2MnO_3 was originally considered to be electrochemically inert, its observed activation has spawned a new class of Li-rich layered compounds that deliver capacities beyond the traditional transition-metal redox limit. Despite progress in our understanding of oxygen redox in Li-rich compounds, the underlying origin of the initial charge capacity of Li_2MnO_3 remains hotly contested. To resolve this issue, we review all possible charge compensation mechanisms including bulk oxygen redox, oxidation of Mn^{4+}, and surface degradation for Li_2MnO_3 cathodes displaying capacities exceeding 350 mAh g^{-1}. Using elemental and orbital selective X-ray spectroscopy techniques, we rule out oxidation of Mn^{4+} and bulk oxygen redox during activation of Li_2MnO_3. Quantitative gas-evolution and titration studies reveal that O_2 and CO_2 release accounted for a large fraction of the observed capacity during activation with minor contributions from reduced Mn species on the surface. These studies reveal that, although Li_2MnO_3 is considered critical for promoting bulk anionic redox in Li-rich layered oxides, Li_2MnO_3 by itself does not exhibit bulk oxygen redox or manganese oxidation beyond its initial Mn^{4+} valence.

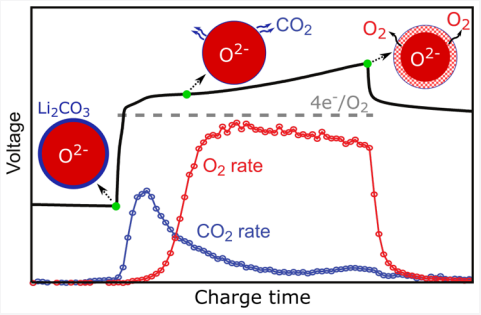

Originally considered electrochemically inactive,[1] Li_2MnO_3 can deliver substantial capacity during charge, as demonstrated by Kalyani et al.[2] Later, Robertson and Bruce[3] revealed how Li_2MnO_3 could be activated through the use of nanosized particles. Indeed, capacities exceeding 300 mAh g^{-1} have been reported during the first charge activation of Li_2MnO_3.[3−10] The large irreversible capacity observed during the first charge is primarily attributed to irreversible oxygen release,[11−16] which presumably activates lattice oxygen redox along with other degradation mechanisms, ultimately leading to severe capacity fade upon cycling.[3,4,6,7,17] Li-rich layered oxides (LR-NMC), derived from Li_2MnO_3 are often regarded as nanocomposites of Li_2MnO_3 and $LiMO_2$ (M = Ni, Mn, Co) components and exhibit a similar first charge activation plateau at 4.5 V vs Li/Li^+.[11,18−21] In fact, a direct correlation observed between the 4.5 V plateau capacity and Li_2MnO_3 content of LR-NMC[22] has been used to quantify the extent of bulk oxygen redox in LR-NMCs.[23] Unlike Li_2MnO_3, LR-NMCs maintain stable cycling performance with high reversible capacities.[24,25] Meanwhile, lattice oxygen redox in LR-NMCs has been supported by numerous O K-edge resonant inelastic X-ray scattering (RIXS) studies,[26−28] with the recent beam exposure studies confirming that the RIXS feature is intrinsic to oxidized lattice oxygen.[29]

While Li_2MnO_3 is regarded as a model compound for describing bulk oxygen redox activity in LR-NMCs, recent RIXS studies did not detect similar spectroscopic signatures of oxidized lattice oxygen in Li_2MnO_3.[30] Additionally, an alternative scenario explaining the origin of anomalous capacity in LR-NMCs has been proposed by Radin et al.[23] According to this new perspective based on first-principle calculations, the reversible formation of molecular oxygen or peroxide ions in combination with Mn^{4+}/Mn^{7+} redox could explain the characteristic electrochemical behavior of LR-NMCs. Meanwhile, the appearance of O K-edge RIXS feature for numerous conventional Mn-free layered oxides questions the role of Li_2MnO_3 in activating lattice oxygen redox in LR-NMCs.[31,32] Understanding the underlying charge compensation mechanism in Li_2MnO_3 is critical for progressing the development of LR-NMCs. This requires answering two fundamental questions: (1) should Li_2MnO_3 be regarded as a model compound describing anionic redox activity and (2) are there any

Received: December 23, 2019
Accepted: January 27, 2020
Published: January 27, 2020

https://dx.doi.org/10.1021/acsenergylett.9b02799
ACS Energy Lett. 2020, 5, 634–641

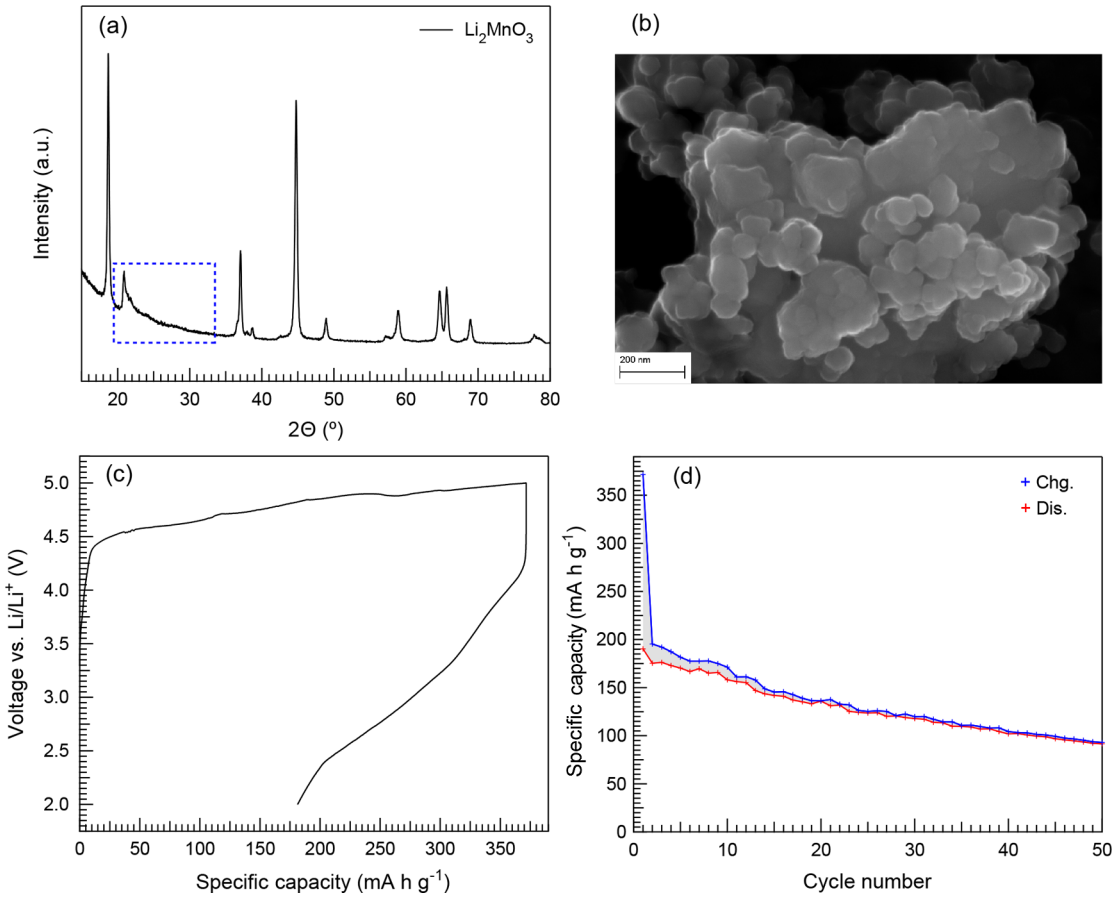

Figure 1. Structure and electrochemistry of Li_2MnO_3. (a) XRD pattern and (b) SEM image showing particles morphology of Li_2MnO_3 synthesized at 600 °C. The first cycle voltage profiles and subsequent cycling performance are shown in (c) and (d), respectively.

alternative charge compensation mechanisms that could explain the electrochemical activity of Li_2MnO_3?

To resolve these issues, we considered all possible charge compensation mechanisms including bulk oxygen redox, Mn^{4+}/Mn^{7+} redox, and surface degradation. Our investigation employed a combination of techniques sensitive to oxygen oxidation (O K-edge RIXS) Mn oxidation (operando Mn K-edge X-ray absorption spectroscopy (XAS)) and gas evolution (differential electrochemical mass spectroscopy (DEMS)). No significant evidence of Mn^{7+} and/or oxidized lattice oxygen were observed by X-ray spectroscopy. Quantitative analysis of the measured gas evolution almost entirely accounted for the observed capacity during the first charge activation, with minor contributions from lattice oxygen redox, carbonate decomposition, and oxidation of reduced Mn species on the surface. Despite being considered critical for understanding bulk oxygen redox activity in LR-NMCs, the parent Li_2MnO_3 itself does not exhibit this exotic charge compensation mechanism. Instead, irreversible oxygen release during activation likely paves the way for other degradation mechanisms, e.g., Mn migration, which will be addressed separately in our future study.

Figure 1a shows the XRD pattern of the as-synthesized material, where all reflections can be indexed in the monoclinic system with the space group $C2/m$.[33] In the layered structure of Li_2MnO_3, the interslab octahedral sites are occupied by Li^+ only, while the octahedral sites within the $[Li_{1/3}Mn_{2/3}]O_2$ slabs are ordered with Li^+ and Mn^{4+} in a ratio of 1:2, which is indicated by the superlattice reflections in the 2θ range from 20 to 34°. However, these superlattice reflections appear convoluted into a broad asymmetric peak as shown in Figure 1a. Previously, the intensity and asymmetry of these superlattice reflections are correlated with the degree of disorder in the stacking sequence of $[Li_{1/3}Mn_{2/3}]O_2$ slabs along the c-direction of the monoclinic lattice.[34] Moreover, the SEM micrograph of the as-synthesized material in Figure 1b reveals the agglomerated primary particles of less than 100 nm in size. Thus, the observed asymmetric superlattice reflection in the XRD pattern confirms an increased degree of stacking faults in the nanocrystalline Li_2MnO_3 synthesized in the present study. Figure 1c demonstrates the voltage profile of Li_2MnO_3 in the first cycle at a rate of C/50 (1 C = 230 mA g^{-1} assumed), while subsequent cycling was performed at C/10. The large irreversible capacity observed during activation, which results in poor Coulombic efficiency of the first cycle, is a characteristic electrochemical feature of Li_2MnO_3. Although cycling performance of Li_2MnO_3 shown in Figure 1d reveals improved Coulombic efficiency for the subsequent cycles, continued degradation leads to significant loss of capacity upon cycling. In other words, the first cycle activation processes likely persist in subsequent cycles but to a much lesser extent. The general consensus in literature is that the first cycle irreversibility in Li_2MnO_3 is due to an irreversible oxygen release.[11−15] Our cycling data indicate that Li_2MnO_3 continues to degas during subsequent cycles, but to a much lesser extent than in the first cycle.

While the irreversible component of the first cycle capacity could be attributed to gas evolution,[11−15] other proposed

https://dx.doi.org/10.1021/acsenergylett.9b02799
ACS Energy Lett. 2020, 5, 634−641

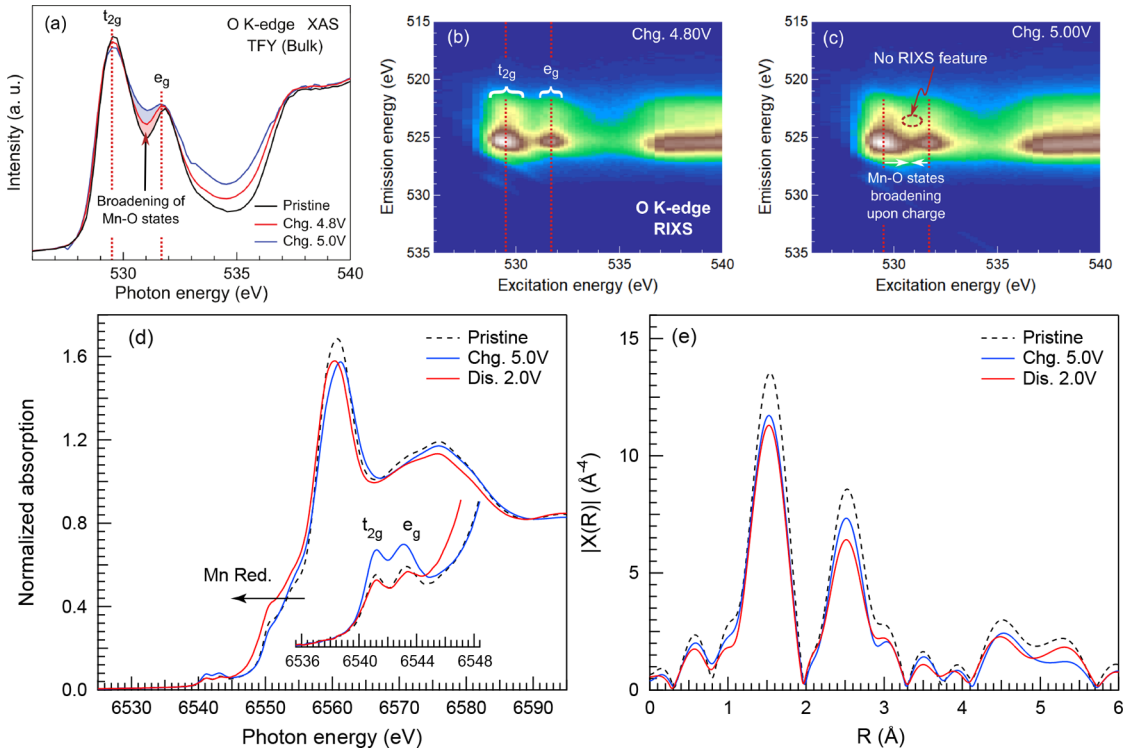

Figure 2. Bulk O and Mn redox activity in Li_2MnO_3. O K-edge TFY XAS data (a), and RIXS maps of Li_2MnO_3 electrodes charged to 4.8 V (b) and 5.0 V (c). Operando Mn K-edge XANES (d) and EXAFS (e) data for charged and discharged states during the first cycle.

charge compensation mechanisms, such as oxidation of Mn^{4+} and/or lattice oxygen redox need to be considered to fully account for the observed total capacity.[23] We first employed O K-edge XAS and RIXS studies to probe bulk redox activity of oxygen anions in Li_2MnO_3. Figure 2a shows the O K-edge spectra in the bulk sensitive total fluorescence yield (TFY) mode for the pristine Li_2MnO_3 and charged electrodes. Corresponding RIXS maps for the charged electrodes are shown in Figure 2b,c. The pre-edge peaks at 529.6 and 531.9 eV are attributed to the hybridization of Mn 3d−O 2p orbitals into t_{2g} and e_g states.[35] At these excitation energies, RIXS maps show two broad density of state (DOS)-like features that are associated with the hybridized Mn−O states. The emergence of RIXS loss feature at 523.5 eVdue to X-ray absorption at 531 eV is regarded as a spectroscopic signature of bulk oxygen redox activity.[27,28,31,36] Our RIXS maps show no evidence of this RIXS feature for the charged electrodes, matching a recent Li_2MnO_3 study,[30] which rules out bulk oxygen redox activity in Li_2MnO_3. The increased weight observed at 531 eV in the O K-edge XAS correlates with broadening of the hybridized t_{2g} and e_g states in the corresponding RIXS maps (Figure 2b,c).

These results are further complemented by a quantitative measure of oxide oxidation using an acid titration of extracted Li_2MnO_3 cathodes. Previous studies on NMC cathode materials have found that O_2 evolves from partially delithiated cathodes when exposed to water if oxygen redox participated in charge compensation. The oxygen evolved from these electrodes is closely related to the well established titrations of lithium peroxide,[37] following the reaction: $Li_2O_2 + H_2O \rightarrow 2LiOH + {}^1/_2O_2$. Therefore, to quantify oxidized oxygen in a state similar to that in Li_2O_2, titrations were used with electrodes extracted at various states of charge (Table S1). An indication of the degree of "reversible" oxygen redox was estimated by comparing electrodes extracted at the top of the first charge and the bottom of the first discharge. Here we have found that these titrations demonstrate minimal contributions from bulk oxygen redox (only 10 mAh g^{-1}), which is in agreement with the lack of spectroscopic feature corresponding to oxidized oxygen in our RIXS measurements (Figure 2b,c).

We then turn to operando Mn K-edge XAS to probe bulk Mn redox activity in Li_2MnO_3 involving Mn^{4+}/Mn^{7+} redox as proposed by Radin et al.[23] However, the experimental verification of the proposed Mn^{4+}/Mn^{7+} redox is considered to be extremely challenging due to fragility of Mn^{7+} under X-ray irradiation.[23] We collected synchrotron XAS data of $KMnO_4$ to inspect the susceptibility of Mn^{7+}-containing oxides to beam damage. Indeed, experimental data could successfully reproduce all major spectral features predicted by calculations from Materials Project[38] (Figure S1). Furthermore, our Mn K-edge XAS data of $KMnO_4$ (Figure S1) are consistent with those reported by others.[5,39,40] These indicate that Mn^{7+}, if present, would be experimentally detected in operando XAS experiments. Notwithstanding this and as an added safeguard, we cycled the pouch cell off-line and exposed to X-rays for data collection only at the predetermined states of charge/discharge, instead of continuously acquiring data by irradiating the cell throughout the entire charge/discharge cycle.

Parts d and e of Figure 2 show operando Mn K-edge X-ray absorption near-edge structure (XANES) and extended X-ray absorption fine structure (EXAFS) data of Li_2MnO_3. At 5.0 V, no clear shift of the main edge beyond that of the pristine state is observed, which rules out the oxidation of Mn^{4+}. The splitting of Mn 3d orbitals into t_{2g} and e_g levels by an octahedral field of the surrounding oxygen can be seen in the pre-edge region, which becomes more intense upon charging to 5.0 V. Meanwhile, reduction in the amplitude of the EXAFS signal observed upon charging to 5.0 V corresponds to increased disorder in the system.[5,10] Indeed, the observed

https://dx.doi.org/10.1021/acsenergylett.9b02799
ACS Energy Lett. 2020, 5, 634−641

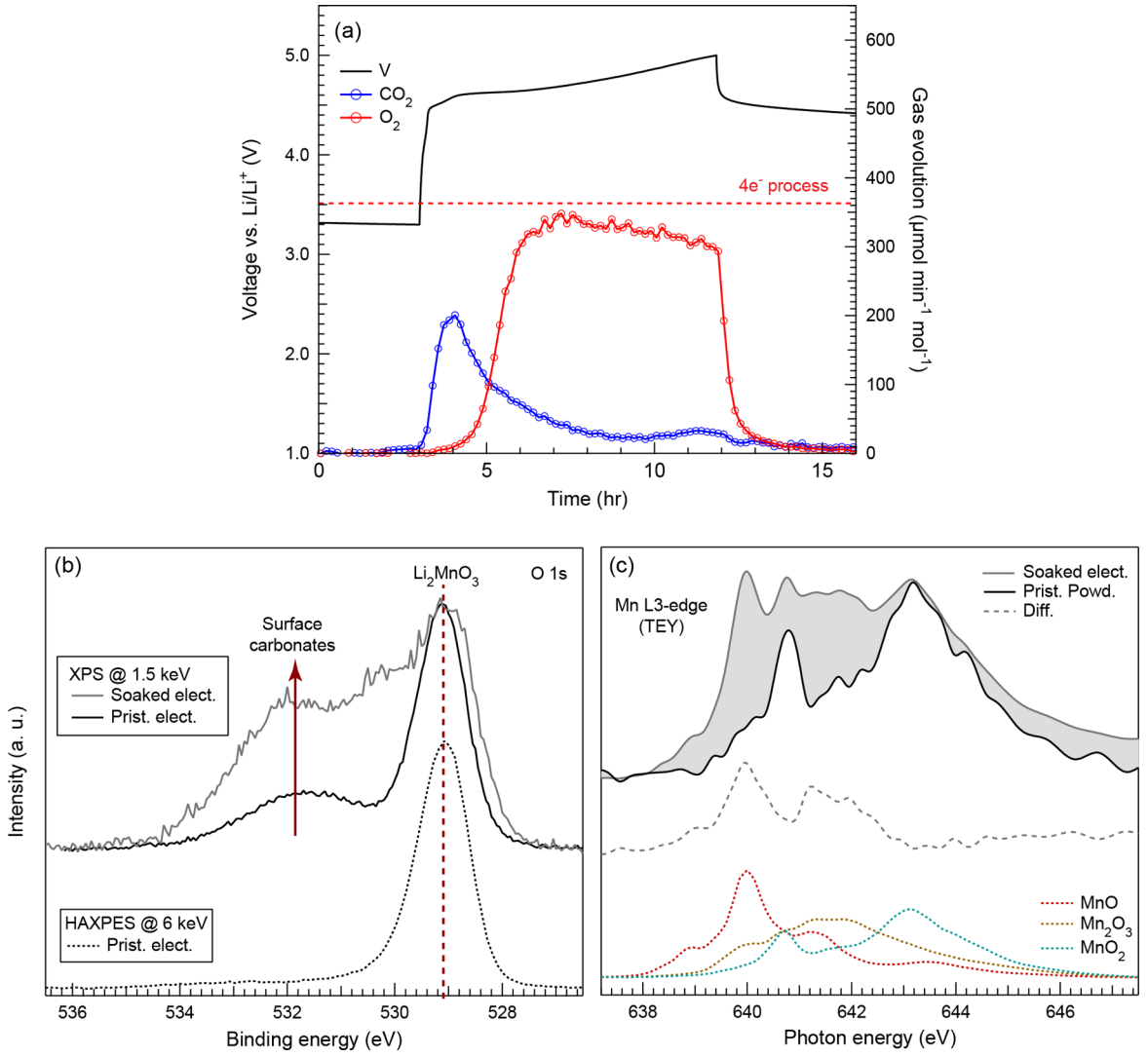

Figure 3. Gas evolution and surface studies of Li_2MnO_3. (a) DEMS for the first charge and (b) XPS/HAXPES data and (c) Mn L3-edge TEY data for the pristine and electrolyte-soaked material.

increase in the intensity of the pre-edge region can now be correlated to major restructuring during activation. This restructuring also likely accounts for the observed broadening of the O K-edge spectral features in Figure 2a–c.[41,42] Upon discharge to 2.0 V, the main edge shifts slightly toward lower energy with respect to that of the charged state, which indicates reduction of Mn^{4+} during lithium reinsertion. To further clarify these trends, we extended our investigation to the second cycle. Similar trends are observed for the charged/discharged states of the second cycle (see Figure S2), except that the second discharge shows even more reduction of Mn^{4+} than the first discharge. These results are in direct agreement with those reported by Croy et al.[10] and confirm that Mn does not oxidize beyond the 4+ oxidation state during charge but undergoes reduction during discharge. These reduced Mn species would then be oxidized during Li extraction on subsequent charge.

Without oxidation of Mn^{4+} and/or reversible participation of lattice oxygen in charge-compensation processes, a remaining possibility is the irreversible oxidation of lattice oxygen to oxygen gas. We employed DEMS to monitor gas evolution from Li_2MnO_3 during the first charge (Figure 3a). Upon application of current, CO_2 was immediately detected, which quickly rose to a sharp peak in evolution rate. As the voltage plateau region was reached, oxygen gas became the dominant evolution product, though CO_2 continued to evolve at a lower rate. Total gas evolved across the first charge summed to be 38 mmol of CO_2 per mol of active material and 113 mmol of O_2 per mol of active material. Note that higher applied currents (20 mA g^{-1}) during DEMS experiments due to instrument availability, as well as variation in the cell design led to the decreased first charge capacity of 177 mAh g^{-1}.

The source of oxygen gas is the formation of oxidized lattice oxygen species followed by gas evolution,[15] as no O_2 evolution results from electrolyte degradation or carbonate oxidation.[37] O_2 evolution from the oxide lattice is a $4e^-$ process, such that the irreversible oxygen contribution to capacity can be calculated from the total oxygen evolved as 125 mAh g^{-1}, or 71% of the total first charge capacity. This oxygen evolved on the first charge accounts for 9.1% of the total oxygen present in the pristine active material. After an initial delay, oxygen evolution proceeds at a rate near that of 4 electrons per molecule oxygen gas released. A 4-electron process involving oxygen molecule would require an oxygen gas release rate of 363 μmol min^{-1} mol^{-1} if oxygen gas accounted for the entire

https://dx.doi.org/10.1021/acsenergylett.9b02799
ACS Energy Lett. 2020, 5, 634–641

first charge capacity. As this is not the case, we examined other capacity contributions.

We note that the CO_2 evolution is remarkably high for a transition metal oxide material. The large quantity of CO_2 evolved (Figure 3c) could originate from a variety of mechanisms, including electrolyte reaction with generated singlet oxygen,[43] surface peroxo species at high voltages, or the oxidation of carbonate impurities in the as-prepared material. To understand the origin of CO_2 evolution, we performed acid titrations and X-ray photoemission spectroscopy (XPS)/hard X-ray photoemission spectroscopy (HAXPES) studies on the extracted electrodes. Acid titrations revealed the presence of 0.4 wt % (6.2 mmol mol^{-1}) of carbonates in the pristine material used for the DEMS study, which is much lower than the total CO_2 evolution observed during galvanostatic charge (38 mmol mol^{-1}). This suggests that electrolyte degradation is the dominant contributor to CO_2 evolution. Interestingly, a titration study on a separate batch of Li_2MnO_3 electrodes both in its pristine state and in the postelectrolyte soak revealed that carbonate content increased by 69% (Table S2) as a result of simply exposing the material to the electrolyte, indicating that the electrolyte largely decomposes and deposits a solid degradation product on the material surface. This is consistent with the XPS O 1s region of the pristine material (Figure 3b) showing a peak between 531.5 and 534 eV binding energy due to the formation of surface carbonates.[44−48] Note the absence of a similar peak in the bulk sensitive HAXPES O 1s region of the pristine material. Meanwhile, Mn L_3-edge TEY XAS data reveal the presence of reduced Mn species on the surface of pristine material (Figure 3c). The amount of surface carbonates and reduced Mn species greatly increased once the electrode is exposed to the electrolyte (Figure 3b,c), which can be attributed to higher surface reactivity of Li_2MnO_3.[49] It is this chemical process that may be the dominant electrolyte degradation mechanism throughout the first charge, although future studies employing isotopic labeling and $^1O_2$ detection are needed to fully understand electrolyte degradation. Nevertheless, our results strongly suggest that the predominant origin for CO_2 evolution is the continuous degradation of the electrolyte to solid surface species, which then oxidize at high voltages to evolve CO_2.

The first charge capacity for Li_2MnO_3 as observed during the DEMS measurement can now be analyzed in terms of the contributions from the processes examined in this study (Table 1). O_2 evolution originating from oxygen oxidation accounts for roughly 70% of the total charge capacity. CO_2 evolution originating from the decomposition of carbonates both present in the initial material as well as formed by electrolyte decomposition accounts for another 10% of the charge capacity. Titrations probing the "reversible" oxygen oxidation (O^{2-}/O^{-}) revealed about 6% contribution to the total charge capacity. We suspect the remaining 14% of the first charge capacity (Table 1) results from a combination of processes including electrolyte decomposition given the high cutoff voltage, as well as the oxidation of reduced Mn species in the near surface region (Figure 3c). Electrolyte decomposition was regarded as a likely source of protons for the previously proposed Li^+/H^+ exchange in Li_2MnO_3.[3,5,50] However, like those previous studies, the X-ray techniques employed in the present study are not directly sensitive to structural protons. Meanwhile, a recent NMR study by Dogan et al.[7] found significant evidence for proton-containing species on the surface of the charged electrode due to side reactions but ruled out insertion of structural protons in Li_2MnO_3.

Table 1. First Charge Capacity Contributions[a]

gas evolution	
O_2	125 mAh g^{-1}
CO_2	17 mAh g^{-1}
"reversible" oxygen redox (OR)	10 mAh g^{-1}
(O_2 + CO_2 + OR)/electrochemistry total	152/177 mAh g^{-1}
other contributions	25 mAh g^{-1}

[a]Capacity contributions as determined using gas evolution and titration techniques compared to the total first charge capacity of the cell run on the DEMS system.

In summary, using the combination of operando Mn K-edge XAS, O K-edge RIXS, XPS/HAXPES, and DEMS, we interpret and quantify the capacity contributions observed during electrochemical activation of Li_2MnO_3. Taken together, the first charge capacity of Li_2MnO_3 originates primarily from oxygen release, with much smaller contributions from reversible lattice oxygen redox, decomposition of surface carbonates and oxidation of reduced Mn species on the surface. Furthermore, our results conclude that Li_2MnO_3 does not exhibit the recently proposed Mn^{4+}/Mn^{7+} redox. For Li_2MnO_3, the octahedrally coordinated Mn prefers not to oxidize beyond 4+ at high voltages consistent with the lack of Mn^{7+} signatures in delithiated LR-NMCs reported thus far. Interestingly, Ceder and co-workers[16] attributed bulk oxygen redox to the labile oxygen states resulting from the Li−O−Li correlations as in Li_2MnO_3. However, the lack of RIXS feature in the charged samples clearly ruled out significant contribution from bulk oxygen redox in Li_2MnO_3. In contrast, the conventional layered oxides without Li−O−Li correlations demonstrated an RIXS feature indicating the onset of bulk oxygen redox at higher degrees of delithiation.[31,32,51] These reports suggest that increased covalency afforded by highly oxidized Ni and Co ions is an important precursor to promoting bulk oxygen redox.[16,52−54] Simply put, the Li_2MnO_3 component in LR-NMC nanocomposites acts as a reservoir of excess Li ions, facilitating capacity beyond the conventional transition-metal (TM) redox by utilizing the inherent TM-O covalency-driven bulk oxygen redox at higher potentials.

■ ASSOCIATED CONTENT

Supporting Information

The Supporting Information is available free of charge at https://pubs.acs.org/doi/10.1021/acsenergylett.9b02799.

Material synthesis and electrochemical details. Additional data includes XANES spectra of reference Mn^{7+} ($KMnO_4$) with Materials Project simulations, operando Mn K-edge XANES of Li_2MnO_3 pouch cells, and oxygen and carbonate titration results (PDF)

■ AUTHOR INFORMATION

Corresponding Author

Louis F. J. Piper − *Department of Physics, Applied Physics, and Astronomy, Binghamton University, New York 13902, United States;* orcid.org/0000-0002-3421-3210; Email: lpiper@binghamton.edu

https://dx.doi.org/10.1021/acsenergylett.9b02799
ACS Energy Lett. 2020, 5, 634−641

Authors

Jatinkumar Rana − *Department of Physics, Applied Physics, and Astronomy, Binghamton University, New York 13902, United States;* orcid.org/0000-0002-3552-2453

Joseph K. Papp − *Department of Chemical and Biomolecular Engineering, University of California, and Energy Storage and Distributed Resources Division, Lawrence Berkeley National Laboratory, Berkeley, California 94720, United States;* orcid.org/0000-0002-7982-6096

Zachary Lebens-Higgins − *Department of Physics, Applied Physics, and Astronomy, Binghamton University, New York 13902, United States*

Mateusz Zuba − *Department of Physics, Applied Physics, and Astronomy, Binghamton University, New York 13902, United States*

Lori A. Kaufman − *Department of Chemical and Biomolecular Engineering, University of California, and Energy Storage and Distributed Resources Division, Lawrence Berkeley National Laboratory, Berkeley, California 94720, United States*

Anshika Goel − *NorthEast Center for Chemical Energy Storage (NECCES), Binghamton University, Binghamton, New York 13902, United States*

Richard Schmuch − *MEET Battery Research Center, Institute of Physical Chemistry, University of Muenster, 48149 Muenster, Germany*

Martin Winter − *Helmholtz-Institute Muenster, IEK-12, Forschungszentrum Juelich GmbH, 48149 Muenster, Germany*

M. Stanley Whittingham − *NorthEast Center for Chemical Energy Storage (NECCES), Binghamton University, Binghamton, New York 13902, United States*

Wanli Yang − *The Advanced Light Source, Lawrence Berkeley National Laboratory, Berkeley, California 94720, United States;* orcid.org/0000-0003-0666-8063

Bryan D. McCloskey − *Department of Chemical and Biomolecular Engineering, University of California, and Energy Storage and Distributed Resources Division, Lawrence Berkeley National Laboratory, Berkeley, California 94720, United States;* orcid.org/0000-0001-6599-2336

Complete contact information is available at: https://pubs.acs.org/10.1021/acsenergylett.9b02799

Author Contributions

[¶]J.R. and J.K.P. had equal contributions.

Notes

The authors declare no competing financial interest.

■ ACKNOWLEDGMENTS

This work was supported as part of the NorthEast Center for Chemical Energy Storage (NECCES), an Energy Frontier Research Center funded by the U.S. Department of Energy, Office of Science, Office of Basic Energy Sciences, under Award No. DE-SC0012583. L.F.J.P and B.D.M. also thank Research Corporation for Science Advancement for funding through the Scialog program. The work at the ALS was supported by the Office of Basic Energy Sciences, of the U.S. Department of Energy, under Contract No. DE-AC02-05CH11231. This research used resources (Beamline 6BMM) of the National Synchrotron Light Source II (NSLS-II), a U.S. Department of Energy (DOE) Office of Science User Facility operated for the DOE Office of Science by Brookhaven National Laboratory under Contract No. DE-SC0012704. The authors gratefully acknowledge Dr. Bruce Ravel for his assistance during XAS experiments at beamline 6BMM of NSLS-II. The authors also acknowledge Diamond Light Source for HAXPES beamtime (Beamline I09) under Proposals No. SI22250-1 and No. SI22148-1 and thank Tien-Lin Lee for his assistance.

■ REFERENCES

(1) Thackeray, M. Manganese oxides for lithium batteries. *Prog. Solid State Chem.* **1997**, *25*, 1−71.

(2) Kalyani, P.; Chitra, S.; Mohan, T.; Gopukumar, S. Lithium metal rechargeable cells using Li2MnO3 as the positive electrode. *J. Power Sources* **1999**, *80*, 103−106.

(3) Robertson, A.; Bruce, P. Mechanism of Electrochemical Activity in Li2MnO3. *Chem. Mater.* **2003**, *15*, 1984−1992.

(4) Yu, D.; Yanagida, K.; Kato, Y.; Nakamura, H. Electrochemical Activities in Li2MnO3. *J. Electrochem. Soc.* **2009**, *156*, A417−A424.

(5) Rana, J.; Stan, M.; Kloepsch, R.; Li, J.; Schumacher, G.; Welter, E.; Zizak, I.; Banhart, J.; Winter, M. Structural Changes in Li2MnO3 Cathode Material for Li-Ion Batteries. *Adv. Energy Mater.* **2014**, *4*, 1300998.

(6) Amalraj, S. F.; Burlaka, L.; Julien, C. M.; Mauger, A.; Kovacheva, D.; Talianker, M.; Markovsky, B.; Aurbach, D. Phase transitions in Li2MnO3 electrodes at various states-of-charge. *Electrochim. Acta* **2014**, *123*, 395−404.

(7) Dogan, F.; Croy, J.; Balasubramanian, M.; Slater, M.; Iddir, H.; Johnson, C.; Vaughey, J.; Key, B. Solid state NMR studies of Li2MnO3 and li-rich cathode materials: Proton insertion, local structure, and voltage fade. *J. Electrochem. Soc.* **2015**, *162*, A235−A243.

(8) Kubota, K.; Kaneko, T.; Hirayama, M.; Yonemura, M.; Imanari, Y.; Nakane, K.; Kanno, R. Direct synthesis of oxygen-deficient Li2MnO3-x for high capacity lithium battery electrodes. *J. Power Sources* **2012**, *216*, 249−255.

(9) Phillips, P. J.; Bareño, J.; Li, Y.; Abraham, D. P.; Klie, R. F. On the Localized Nature of the Structural Transformations of Li2MnO3 Following Electrochemical Cycling. *Adv. Energy Mater.* **2015**, *5*, 1501252.

(10) Croy, J.; Park, J.; Dogan, F.; Johnson, C.; Key, B.; Balasubramanian, M. First-Cycle Evolution of Local Structure in Electrochemically Activated Li2MnO3. *Chem. Mater.* **2014**, *26*, 7091−7098.

(11) Lu, Z.; Dahn, J. Understanding the Anomalous Capacity of Li/Li[NixLi(1/32x/3)Mn(2/3x/3)O2 Cells Using In Situ X-Ray Diffraction and Electrochemical Studies. *J. Electrochem. Soc.* **2002**, *149*, A815.

(12) Kim, J.-S.; Johnson, C.; Vaughey, J.; Thackeray, M.; Hackney, S.; Yoon, W.; Grey, C. Electrochemical and structural properties of xLi2MO 3·(1-x)LiMn0.5Ni0.5O2 electrodes for lithium batteries (M = Ti, Mn, Zr; O x 0.3). *Chem. Mater.* **2004**, *16*, 1996−2006.

(13) Johnson, C.; Kim, J.-S.; Lefief, C.; Li, N.; Vaughey, J.; Thackeray, M. The significance of the Li2MnO3 component in 'composite' xLi2MnO3*(1-x)LiMn0.5Ni0.5O2 electrodes. *Electrochem. Commun.* **2004**, *6*, 1085−1091.

(14) Armstrong, A.; Holzapfel, M.; Novák, P.; Johnson, C.; Kang, S.-H.; Thackeray, M.; Bruce, P. Demonstrating oxygen loss and associated structural reorganization in the lithium battery cathode Li[Ni0.2Li0.2Mn0.6]O2. *J. Am. Chem. Soc.* **2006**, *128*, 8694−8698.

(15) Chen, H.; Islam, M. S. Lithium extraction mechanism in Li-rich Li2MnO3involving oxygen hole formation and dimerization. *Chem. Mater.* **2016**, *28*, 6656−6663.

(16) Seo, D.-H.; Lee, J.; Urban, A.; Malik, R.; Kang, S.; Ceder, G. The structural and chemical origin of the oxygen redox activity in layered and cation-disordered Li-excess cathode materials. *Nat. Chem.* **2016**, *8*, 692−697.

(17) Yan, P.; Xiao, L.; Zheng, J.; Zhou, Y.; He, Y.; Zu, X.; Mao, S. X.; Xiao, J.; Gao, F.; Zhang, J.-G.; Wang, C.-M. Probing the Degradation Mechanism of Li2MnO3 Cathode for Li-Ion Batteries. *Chem. Mater.* **2015**, *27*, 975−982.

(18) Johnson, C.; Li, N.; Lefief, C.; Thackeray, M. Anamolous capacity and cycling stability of xLi2MnO3*(1-x)LiMO2 electrodes (M = Mn,Ni,Co) in lithium batteries at 50C. *Electrochem. Commun.* **2007**, *9*, 787−795.
(19) Thackeray, M.; Kang, S.-H.; Johnson, C.; Vaughey, J.; Benedek, R.; Hackney, S. Li2MnO3-stabilized LiMO2 (M= Mn, Ni, Co) electrodes for lithium-ion batteries. *J. Mater. Chem.* **2007**, *17*, 3112−3125.
(20) Rana, J.; Kloepsch, R.; Li, J.; Scherb, T.; Schumacher, G.; Winter, M.; Banhart, J. On the structural integrity and electrochemical activity of a 0.5Li2MnO3*0.5LiCoO2 cathode material for lithium-ion batteries. *J. Mater. Chem. A* **2014**, *2*, 9099−9110.
(21) Rana, J.; Kloepsch, R.; Li, J.; Stan, M.; Schumacher, G.; Winter, M.; Banhart, J. Structural Changes in a Li-Rich 0.5Li2MnO3 * 0.5LiMn0.4Ni0.4Co0.2O2 Cathode Material for Li-Ion Batteries: A Local Perspective. *J. Electrochem. Soc.* **2016**, *163*, A811−A820.
(22) Teufl, T.; Strehle, B.; Müller, P.; Gasteiger, H.; Mendez, M. Oxygen Release and Surface Degradation of Li- and Mn-Rich Layered Oxides in Variation of the Li2MnO3 Content. *J. Electrochem. Soc.* **2018**, *165*, A2718−A2731.
(23) Radin, M.; Vinckeviciute, J.; Seshadri, R.; Van der Ven, A. Manganese oxidation as the origin of the anomalous capacity of Mn-containing Li-excess cathode materials. *Nature Energy* **2019**, *4*, 639−646.
(24) Qiu, B.; Zhang, M.; Wu, L.; Wang, J.; Xia, Y.; Qian, D.; Liu, H.; Hy, S.; Chen, Y.; An, K.; Zhu, Y.; Liu, Z.; Meng, Y. Gas−solid interfacial modification of oxygen activity in layered oxide cathodes for lithium-ion batteries. *Nat. Commun.* **2016**, *7*, 12108.
(25) Pimenta, V.; Sathiya, M.; Batuk, D.; Abakumov, A. M.; Giaume, D.; Cassaignon, S.; Larcher, D.; Tarascon, J. M. Synthesis of Li-Rich NMC: A Comprehensive Study. *Chem. Mater.* **2017**, *29*, 9923−9936.
(26) Luo, K.; Roberts, M. R.; Hao, R.; Guerrini, N.; Pickup, D. M.; Liu, Y.-s.; Edström, K.; Guo, J.; Chadwick, A. V.; Duda, L. C.; Bruce, P. G. Charge-compensation in 3d-transition-metal-oxide intercalation cathodes through the generation of localized electron holes on oxygen. *Nat. Chem.* **2016**, *8*, 684.
(27) Gent, W.; et al. Coupling between oxygen redox and cation migration explains unusual electrochemistry in lithium-rich layered oxides. *Nat. Commun.* **2017**, *8*, 2091.
(28) Xu, J.; Sun, M.; Qiao, R.; Renfrew, S. E.; Ma, L.; Wu, T.; Hwang, S.; Nordlund, D.; Su, D.; Amine, K.; Lu, J.; McCloskey, B. D.; Yang, W.; Tong, W. Elucidating anionic oxygen activity in lithium-rich layered oxides. *Nat. Commun.* **2018**, *9*, 947.
(29) Lebens-Higgins, Z.; Vinckeviciute, J.; Wu, J.; Faenza, N.; Li, Y.; Sallis, S.; Pereira, N.; Meng, Y.; Amatucci, G.; Van Der Ven, A.; Yang, W.; Piper, L. Distinction between Intrinsic and X-ray-Induced Oxidized Oxygen States in Li-Rich 3d Layered Oxides and LiAlO2. *J. Phys. Chem. C* **2019**, *123*, 13201−13207.
(30) Massel, F.; Hikima, K.; Rensmo, H.; Suzuki, K.; Hirayama, M.; Xu, C.; Younesi, R.; Liu, Y.-S.; Guo, J.; Kanno, R.; Hahlin, M.; Duda, L.-C. Excess Lithium in Transition Metal Layers of Epitaxially Grown Thin Film Cathodes of Li 2 MnO 3 Leads to Rapid Loss of Covalency during First Battery Cycle. *J. Phys. Chem. C* **2019**, *123*, 28519−28526.
(31) Lebens-Higgins, Z.; et al. Revisiting the charge compensation mechanisms in LiNi 0.8 Co 0.2y Al y O 2 systems. *Mater. Horiz.* **2019**, *6*, 2112−2123.
(32) Li, N.; Sallis, S.; Papp, J.; Wei, J.; McCloskey, B.; Yang, W.; Tong, W. Unraveling the Cationic and Anionic Redox Reactions in a Conventional Layered Oxide Cathode. *ACS Energy Letters* **2019**, *4*, 2836−2842.
(33) Strobel, P.; Lambert-Andron, B. Crystallographic and magnetic structure of Li2MnO3. *J. Solid State Chem.* **1988**, *75*, 90−98.
(34) Boulineau, A.; Croguennec, L.; Delmas, C.; Weill, F. Structure of Li2MnO3 with different degrees of defects. *Solid State Ionics* **2010**, *180*, 1652−1659.
(35) Liang, Y.; Prendergast, D. Quantum many-body effects in x-ray spectra efficiently computed using a basic graph algorithm. *Phys. Rev. B: Condens. Matter Mater. Phys.* **2018**, *97*, 205127.
(36) Yang, W.; Devereaux, T. Anionic and cationic redox and interfaces in batteries: Advances from soft X-ray absorption spectroscopy to resonant inelastic scattering. *J. Power Sources* **2018**, *389*, 188−197.
(37) Renfrew, S.; McCloskey, B. Quantification of Surface Oxygen Depletion and Solid Carbonate Evolution on the First Cycle of LiNi 0.6 Mn 0.2 Co 0.2 O 2 Electrodes. *ACS Applied Energy Materials* **2019**, *2*, 3762−3772.
(38) Jain, A.; Ong, S.; Hautier, G.; Chen, W.; Richards, W.; Dacek, S.; Cholia, S.; Gunter, D.; Skinner, D.; Ceder, G.; Persson, K. Commentary: The materials project: A materials genome approach to accelerating materials innovation. *APL Mater.* **2013**, *1*, 011002.
(39) Christensen, A.; Hansen, P.; Lehmann, M. Isotope Effects in the Bonds of a-CrOOH and a-CrOOD. *J. Solid State Chem.* **1977**, *21*, 325−329.
(40) Yamamoto, T. Assignment of pre-edge peaks in K-edge x-ray absorption spectra of 3d transition metal compounds: electric dipole or quadrupole? *X-Ray Spectrom.* **2008**, *37*, 572−584.
(41) Wang, D.; Liu, L.; Sun, X.; Sham, T.-K. T.-K. Observation of lithiation-induced structural variations in TiO 2 nanotube arrays by X-ray absorption fine structure. *J. Mater. Chem. A* **2015**, *3*, 412−419.
(42) Gautam, S.; Das, A.; Ojha, S.; Shukla, D.; Phase, D.; Singh, F. Electronic structure modification and Fermi level shifting in niobium-doped anatase titanium dioxide thin films: a comparative study of NEXAFS, work function and stiffening of phonons. *Phys. Chem. Chem. Phys.* **2016**, *18*, 3618−3627.
(43) Wandt, J.; Freiberg, A. T.; Ogrodnik, A.; Gasteiger, H. Singlet oxygen evolution from layered transition metal oxide cathode materials and its implications for lithium-ion batteries. *Mater. Today* **2018**, *21*, 825−833.
(44) Grenier, A.; Liu, H.; Wiaderek, K.; Lebens-Higgins, Z.; Borkiewicz, O.; Piper, L.; Chupas, P.; Chapman, K. Reaction Heterogeneity in LiNi0.8Co0.15Al0.05O2 Induced by Surface Layer. *Chem. Mater.* **2017**, *29*, 7345−7352.
(45) Lebens-Higgins, Z.; Sallis, S.; Faenza, N.; Badway, F.; Pereira, N.; Halat, D.; Wahila, M.; Schlueter, C.; Lee, T.-L.; Yang, W.; Grey, C.; Amatucci, G.; Piper, L. Evolution of the Electrode−Electrolyte Interface of LiNi0.8Co0.15Al0.05O2 Electrodes Due to Electrochemical and Thermal Stress. *Chem. Mater.* **2018**, *30*, 958−969.
(46) Edström, K.; Gustafsson, T.; Thomas, J. O. The cathode-electrolyte interface in the Li-ion battery. *Electrochim. Acta* **2004**, *50*, 397−403.
(47) El Ouatani, L.; Dedryvre, R.; Siret, C.; Biensan, P.; Reynaud, S.; Iraţabal, P.; Gonbeau, D. The Effect of Vinylene Carbonate Additive on Surface Film Formation on Both Electrodes in Li-Ion Batteries. *J. Electrochem. Soc.* **2009**, *156*, A103.
(48) Dahéron, L.; Dedryvère, R.; Martinez, H.; Ménétrier, M.; Denage, C.; Delmas, C.; Gonbeau, D. Electron Transfer Mechanisms upon Lithium Deintercalation from LiCoO 2 to CoO 2 Investigated by XPS. *Chem. Mater.* **2008**, *20*, 583−590.
(49) Quesne-Turin, A.; Flahaut, D.; Croguennec, L.; Vallverdu, G.; Allouche, J.; Charles-Blin, Y.; Chotard, J.-N.; Ménétrier, M.; Baraille, I. Surface Reactivity of Li2MnO3: First-Principles and Experimental Study. *ACS Appl. Mater. Interfaces* **2017**, *9*, 44222−44230.
(50) Robertson, A.; Bruce, P. The origin of electrochemical activity in Li2MnO3. *Chem. Commun.* **2002**, 2790−2791.
(51) Zhang, J.-N.; et al. Trace doping of multiple elements enables stable battery cycling of LiCoO2 at 4.6 V. *Nature Energy* **2019**, *4*, 594−603.
(52) McCalla, E.; Abakumov, A.; Saubanère, M.; Foix, D.; Berg, E.; Rousse, G.; Doublet, M.; Gonbeau, D.; Novák, P.; Van Tendeloo, G.; Dominko, R.; Tarascon, J.-M. Visualization of O-O peroxo-like dimers in high-capacity layered oxides for Li-ion batteries. *Science (Washington, DC, U. S.)* **2015**, *350*, 1516−21.
(53) Xie, Y.; Saubanère, M.; Doublet, M.-L. Requirements for reversible extra-capacity in Li-rich layered oxides for Li-ion batteries. *Energy Environ. Sci.* **2017**, *10*, 266−274.
(54) Zhao, E.; Zhang, M.; Wang, X.; Hu, E.; Liu, J.; Yu, X.; Olguin, M.; Wynn, T.; Meng, Y.; Page, K.; Wang, F.; Li, H.; Yang, X.-Q.;

Huang, X.; Chen, L. Local structure adaptability through multi cations for oxygen redox accommodation in Li-Rich layered oxides. *Energy Storage Materials* **2020**, *24*, 384−393.

https://dx.doi.org/10.1021/acsenergylett.9b02799
ACS Energy Lett. 2020, 5, 634−641